Reviewer 1

This manuscript evaluates the sensitivity of Arctic mixed-phase cloud simulations to ice microphysical modifications in the WDM6 scheme using WRF for the M-PACE case. The comparison between the original WDM6 scheme, the full WDM6_ICE scheme, and intermediate sensitivity experiments is valuable. The study addresses an important problem: how bulk microphysics schemes partition water between liquid and ice phases in Arctic mixed-phase clouds, and whether modifications developed or tested in other regimes behave consistently under Arctic conditions.

The manuscript is generally well structured and contains useful diagnostics, especially the decomposition into ice-shape and ice-nucleation modifications. The paper is clearly written and easy to follow. However, several aspects require clarification before the conclusions can be fully supported. My main concerns are the justification and generality of the selected case, the model-observation sampling strategy for aircraft comparison, the vertical displacement of simulated cloud structure, and the strength of the regime-dependent interpretation. I therefore recommend major revision.

: We sincerely appreciate the reviewer's careful reading and constructive comments. The manuscript has been revised accordingly, and detailed responses are provided under each comment below.

Major comments

1. The selection of the 9–10 October 2004 M-PACE case should be better justified. Although M-PACE is a well-established benchmark for Arctic mixed-phase cloud studies, the manuscript should clarify why this particular case is suitable for evaluating regime dependent responses of WDM6_ICE. In particular, the authors should discuss whether the relatively narrow and warm subzero cloud-temperature range and the single-layer boundary-layer structure make this case representative of Arctic MPCs more broadly, or whether the conclusions should be interpreted as case-specific.

: We thank the reviewer for the opportunity to clarify the case-selection rationale. The 9–10 October 2004 single-layer stratocumulus sub-case is suited to the mechanistic decomposition pursued here for two reasons. First, the single-layer, well-mixed structure removes the complications of multilayer cloud systems and provides a clean testbed for isolating the microphysical pathways (Klein et al., 2009). Second, its cold subzero cloud-temperature range (about −15 to −10 ℃), which lies outside the Hallett–Mossop window, together with low ice-nucleating particle concentrations and shallow boundary-layer coupling, is thermodynamically distinct from the mid-latitude precipitation cases of Park and Lim (2023), making it a suitable Arctic counterpart for evaluating whether the WDM6_ICE modifications respond consistently across regimes. We interpret the conclusions within this scope rather than as broadly representative of all Arctic mixed-phase clouds. Accordingly, we have added a paragraph to the Conclusions stating that the findings are based on a single M-PACE case and that their quantitative generality across the broader range of Arctic mixed-phase conditions remains to be tested with additional cases in future work, with consistent statements in the Introduction and the case description (Section 2.2). The broader within-Arctic

generality is discussed in our response to Major Comment 5.

2. The comparison with aircraft observations should be more carefully justified. The manuscript appears to compare aircraft profiles with model profiles averaged over a flight region rather than strictly collocated along the aircraft track and sampling time. Since Arctic MPCs can exhibit substantial spatial variability, regional averaging may smooth cloud structures and affect the diagnosed peak height and magnitude of LWC/IWC. The authors should either provide a track-collocated model–observation comparison or justify why regional averaging is more appropriate.

: We thank the reviewer for this point. We have replaced the region-averaged comparison with a track-collocated sampling along Flight 10a, and Figures 3 and 6 have been updated accordingly. For each D03 grid cell crossed by the flight track during 01:10–02:00 UTC, the model profiles are sampled and averaged, using the hourly model outputs at 01:00 and 02:00 UTC, and then binned onto the observation altitude grid. During this window the aircraft sampled the cloud by executing repeated vertical spirals over a confined area near Barrow (McFarquhar et al., 2007), so the observed profile is itself a composite of multiple profiles over that area rather than a single instantaneous transect. Averaging the model over the same set of track cells and time window is therefore the consistent counterpart to the observed profile. The hourly model output makes an instantaneous, point-by-point collocation along the 1-Hz track infeasible, but restricting the model sample to the track cells limits the spatial smoothing that a broader regional average would introduce. The Methods (Section 2.3) have been revised to describe this track-cell sampling, and the figure captions now state that the model profiles are sampled along the track between 01:00 and 02:00 UTC.

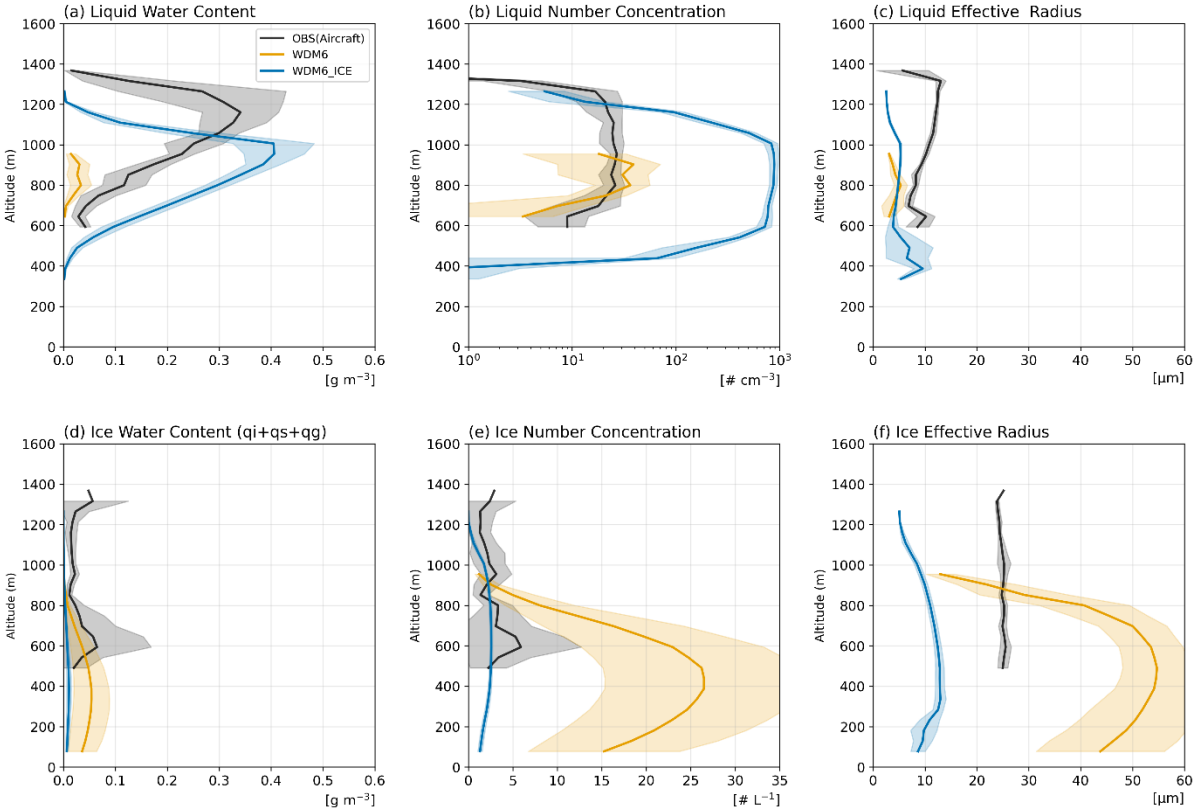

Figure R1: Vertical profiles of cloud microphysical properties along the flight track (Flight 10a). Panels show (a-c) liquid water content (LWC), number concentration, and effective radius, and (d-f) ice water content (IWC: q_i+q_s+q_g), number concentration, and effective radius. Black lines represent aircraft observations (01:10–02:00 UTC 10 October 2004) with gray shading indicating ±1 standard deviation (σ). Colored lines denote model simulations sampled along the track between the 01:00–02:00 UTC, WDM6 (orange) and WDM6_ICE (blue) with shading indicating ±1σ across the track grid cells.

3. The vertical location of the simulated cloud layer appears biased low relative to the aircraft observations. For example, the observed LWC peaks around 1200 m, whereas WDM6_ICE peaks around 1000 m and WDM6 even lower. This vertical displacement may affect the evaluation of LWC/IWC magnitude, phase partitioning, and radiative coupling. The authors should discuss possible causes, such as boundary-layer height, inversion height, thermodynamic profile biases, sampling strategy, and assess whether this vertical mismatch influences the main conclusions.

: We thank the reviewer for this important point. We have expanded the thermodynamic-profile figure as show in Fig. R2 (Fig. S3 in the original manuscript) to show temperature, potential temperature, relative humidity, and water vapor mixing ratio together with the diagnosed cloud-top heights at BAR, using the radiosondes on 9 October 2004. The observed cloud top is near 1371 m, while all simulations are lower (1162 m in WDM6_ICE and 873 m in WDM6). The potential temperature profiles show that the modelled inversion and boundary-layer top are lower than observed, and this bias is already present in the ERA5 boundary conditions (cloud top 1182 m). Because all experiments share the same ERA5 forcing and boundary-layer scheme, this low bias is common to every configuration and does not affect the relative comparison of the microphysical sensitivities that is the focus of this study. Consistent with this, the

microphysical sensitivity hierarchy is preserved when the boundary-layer scheme is changed (Fig. S4 in the original manuscript), confirming that the relative differences do not depend on a particular boundary-layer configuration. We have added a paragraph discussing this in Section 4.4.

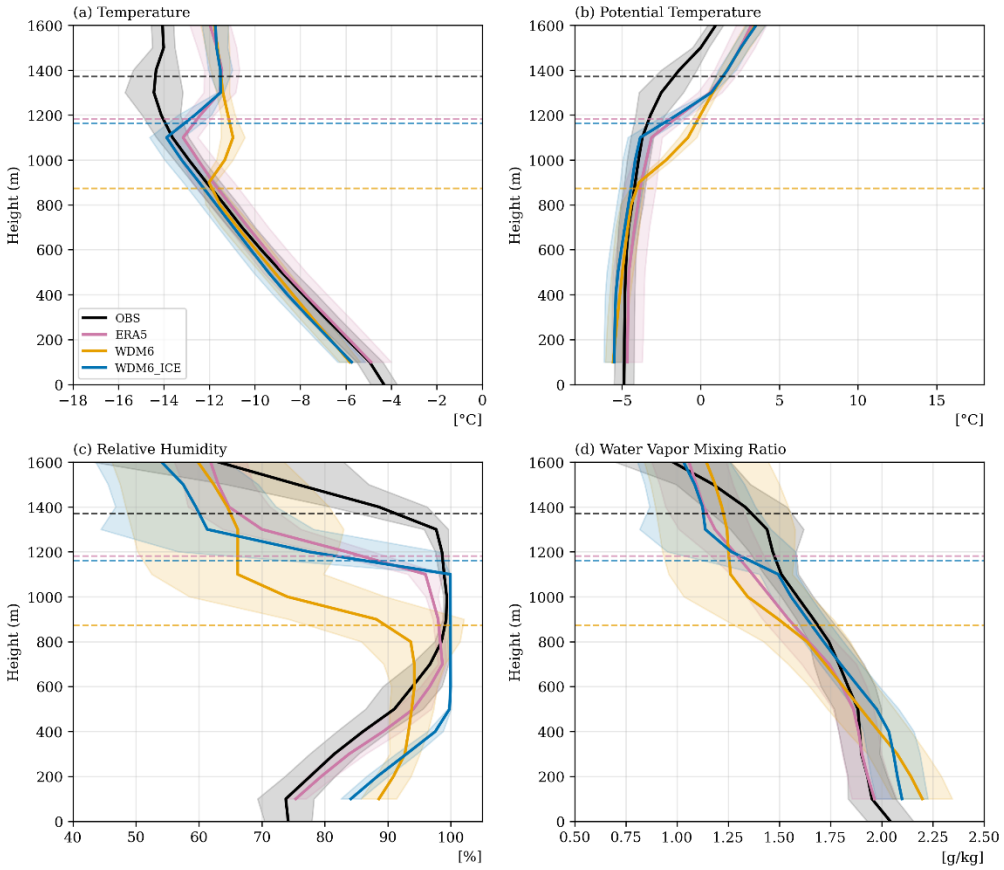

Figure R2: Vertical profiles at BAR averaged over three times (approximately 12:00, 17:00, and 23:00 UTC) on 9 October 2004 of (a) temperature, (b) potential temperature, (c) relative humidity, and (d) water vapor mixing ratio. Black lines show the radiosonde observations (launched at 11:50, 17:00, and 23:02 UTC) and pink, orange, and blue lines show ERA5, WDM6, and WDM6_ICE, with shading indicating ±1σ across the three times. The dashed horizontal lines mark the diagnosed cloud-top height for each profile (same colors as the lines).

4. The role of precipitation and sedimentation is not sufficiently discussed. Since the manuscript argues that WDM6_ICE shifts the ice budget from cloud ice toward snow and modifies liquid-to-ice/snow conversion pathways, changes in snowfall, precipitation flux, and sedimentation should be examined or at least discussed. These processes directly affect cloud water content, cloud lifetime, and the interpretation of LWP/IWP differences. The authors should clarify whether precipitation/sedimentation differs among experiments and whether it contributes to the reduced total water path and altered phase partitioning.

: We thank the reviewer for this point. To examine the role of precipitation and sedimentation, we added the autoconversion of cloud ice to snow (Psaut) and the accretion of cloud ice by snow (Psaci) as a new panel (d) to Fig. 5. We also examined the surface precipitation rate and the accumulated snowfall for all five experiments, shown in Fig. S4, and we have added the accumulated surface precipitation (PRECIP) to Table 3. To document the accompanying shift of the in-cloud ice budget from cloud ice toward snow, we also decomposed the total IWC along the flight track into cloud ice, snow, and graupel mixing ratios for all five experiments (Fig. S3; Fig. R5 of this response). A discussion has been added to Section 4.1.
The precipitation, which is almost entirely snowfall under the subzero conditions of this case, differs substantially among the configurations. WDM6 and WDM6_IN produce the largest amounts (about 2.6 mm), whereas WDM6_ICE produces the smallest (0.39 mm), with WDM6_SP and WDM6_SP_IN intermediate (about 0.9 mm). In WDM6, strong vapor deposition onto cloud ice (Pidep; Fig. 5c) generates abundant cloud ice that is efficiently converted to snow (Psaut; Fig. 5d) and removed by sedimentation. In WDM6_ICE, the suppression of Pidep limits cloud ice and weakens Psaut (Fig. 5d), so the precipitation is much smaller.
These precipitation differences contribute to the total water path (TWP) differences among the configurations: the configurations with the largest precipitation (WDM6, WDM6_IN) remove column water most efficiently through deposition-grown snow and sedimentation, which lowers their TWP, whereas WDM6_ICE produces little snow and retains a persistent liquid layer with a higher TWP. Regarding the phase partitioning, the reduced precipitation in WDM6_ICE and the shift of the in-cloud ice composition toward snow both accompany the suppression of vapor deposition onto cloud ice, so we describe them as linked aspects of the same change in ice microphysics rather than assigning a causal direction, which the present experiments cannot isolate. We also note that the snow-dominated ice budget described in Section 3.1 refers to the in-cloud composition, in which snow exceeds cloud ice within the residual ice phase, and is distinct from the surface snowfall rate. Figure S3 illustrates this in-cloud composition for each configuration. In WDM6 the residual ice is carried almost entirely by cloud ice, whereas in WDM6_ICE cloud ice becomes negligible and snow dominates the residual ice. In WDM6_IN the cloud-ice mass is only slightly lower than in WDM6 and is offset by a corresponding increase in snow, so the total ice content is largely conserved, consistent with the redistribution rather than reduction of ice by the nucleation modification.

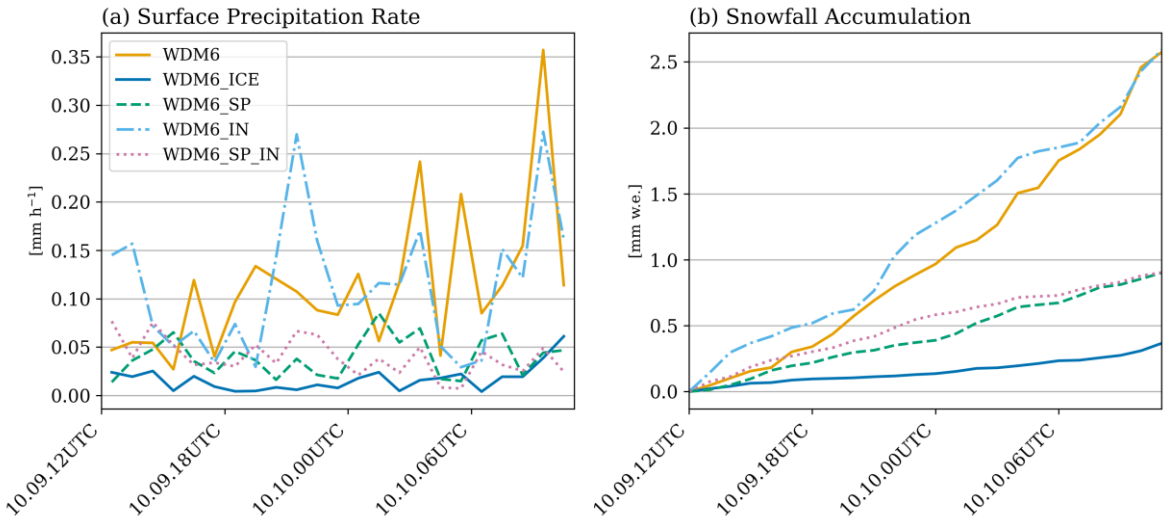

Figure R3: (a) Surface precipitation rate and (b) accumulated snowfall (water equivalent) at BAR over 12:00 UTC 9 October – 11:00 UTC 10 October 2004 for WDM6, WDM6_ICE, WDM6_SP, WDM6_IN, and WDM6_SP_IN.

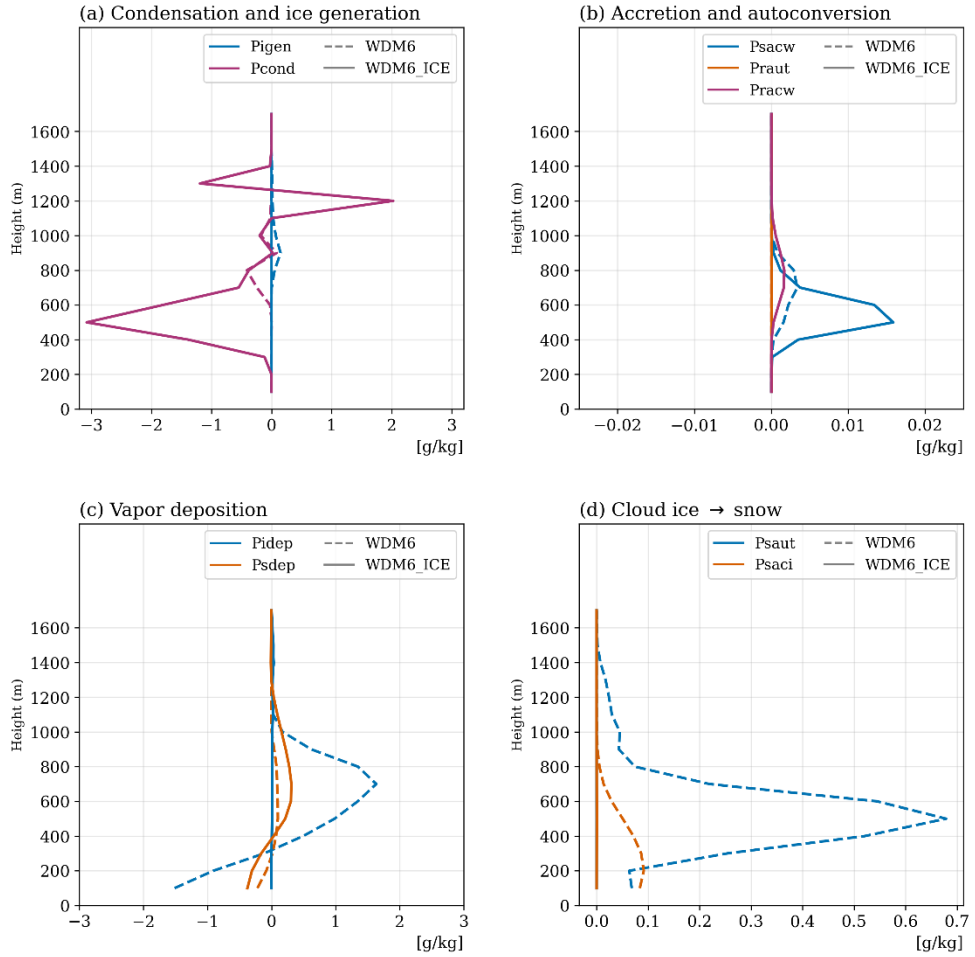

Figure R4: Time-averaged (12:00 UTC 9 October – 11:00 UTC 10 October 2004) vertical profiles of microphysical process rates at BAR: (a) condensation and ice generation (Pigen, Pcond), (b) accretion and autoconversion (Psacw, Praut, Pracw), (c) vapor deposition (Pidep, Psdep), and (d) cloud ice to snow conversion (Psaut, Psaci). Dashed lines represent WDM6, and solid lines represent WDM6_ICE. Note that negative values in (a) indicate evaporation.

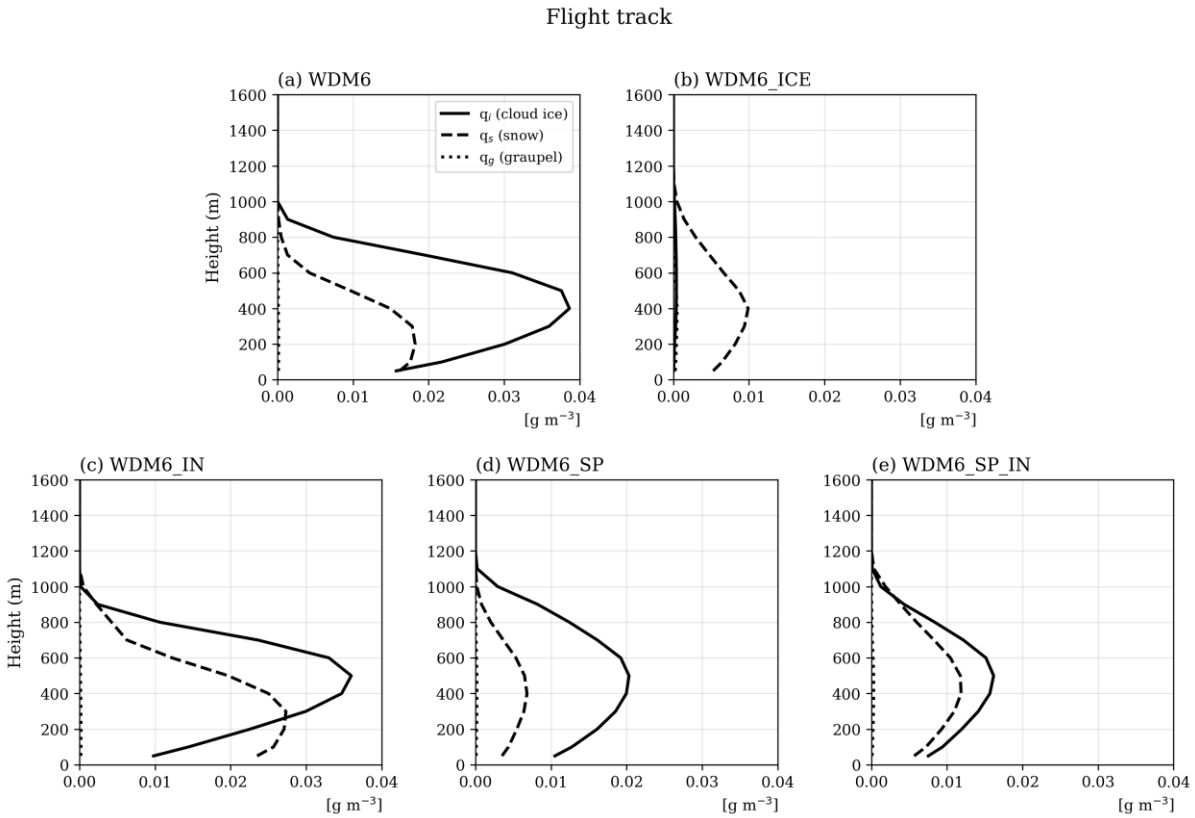

Figure R5: Decomposition of the total IWC along the flight track (Figure 3d) into cloud ice (q_i, solid), snow (q_s, dashed), and graupel (q_g, dotted) mixing ratios for (a) WDM6, (b) WDM6_ICE, (c) WDM6_IN, (d) WDM6_SP, and (e) WDM6_SP_IN, sampled between 01:00 and 02:00 UTC 10 October 2004.

5. The conclusion that the response is "regime-dependent" should be stated more cautiously. The present evidence is based on a single M-PACE case with a relatively narrow cloud-temperature range of approximately −15 to −10 °C. The authors themselves note that this temperature range lies outside the Hallett–Mossop secondary ice production window. Therefore, the strong ice suppression in WDM6_ICE may be partly case-dependent or temperature-regime-dependent rather than generally representative of Arctic MPCs. Other Arctic cases, for example cases within the Hallett– Mossop temperature window or cases with stronger primary nucleation, could produce different responses. The authors should either provide additional cases/sensitivity tests or soften the generality of the regime-dependent conclusion.

: We agree, and have softened the generality of the regime-dependent interpretation to reflect its single-case basis on the Arctic side. The interpretation is retained but explicitly qualified as resting on single-case evidence, since Park and Lim (2023) examined multiple mid-latitude ICE-POP cases whereas the present study examines a single Arctic single-layer case. Section 4.2 has been revised from "This asymmetric response demonstrates that the sensitivity of microphysical parameterizations to environmental conditions is itself regime-dependent: modifications that produce quantitative corrections in one regime can trigger qualitative shifts in cloud ice budget structure in another." to "This asymmetric response indicates regime-dependent behavior of the microphysical modifications, although it is based on a single Arctic case

and should be interpreted with caution. Whether the contrast persists across the broader range of Arctic mixed-phase conditions remains to be tested in future work." Consistent single-case statements have been added to the Abstract, the Introduction, and the case description (Section 2.2), and the Conclusions now note that additional cases, including cases within the Hallett–Mossop temperature window or with stronger primary nucleation as the reviewer suggests, are needed to test this interpretation.

Minor comments

1. In Fig. 1b, please clarify what the color shading over the ocean represents. If this is a MODIS visible/true-color image rather than a quantitative variable, this should be stated explicitly in the caption. If a color scale is used, the variable and units should be provided.

: The color shading over the ocean and land in Fig. 1b shows ocean depth and land elevation from the GEBCO_2023 grid (GEBCO Compilation Group, 2023), as given by the color bar (Depth and Elevation in meters), overlaid with the grayscale MODIS visible image. We have revised the Fig. 1 caption to state this and added the GEBCO_2023 grid to the Data Availability

2. Please clarify that the 20 levels below 800 hPa are included within the total 50 vertical levels, rather than additional levels.

: The 20 levels below 800 hPa are part of the total of 50 vertical levels, not additional levels. We have clarified this in Section 2.3 and Table 1, and unified the terminology to "levels" throughout.

3. Please indicate in the Fig. 2 caption that the plotted spatial fields correspond to D03, if that is the case.

: The spatial fields in Fig. 2 correspond to domain D03. We have added this to the Fig. 2 caption.

4. In Fig. 6, the height of peak LWC appears to shift upward from WDM6 to WDM6_ICE as supercooled liquid water increases. The authors should briefly explain whether this reflects changes in boundary-layer depth, cloud-top radiative cooling, thermodynamic structure, or microphysical suppression of ice deposition.

: The upward shift of the LWC peak from WDM6 to WDM6_ICE reflects the higher simulated boundary layer and cloud top in WDM6_ICE. As shown in the thermodynamic profiles (Fig. S5) and the boundary-layer height (Fig. 4c), the inversion and cloud top are higher in WDM6_ICE (cloud top about 1160 m) than in WDM6 (about 870 m), and the LWC peak, which forms near cloud top below the inversion, shifts upward accordingly. The other factors raised by the reviewer are consistent with this picture: the microphysical suppression of ice deposition allows WDM6_ICE to maintain more supercooled liquid and a colder cloud top, and the associated stronger cloud-top

radiative cooling is consistent with a deeper, better-mixed boundary layer, which in stratocumulus-topped layers is driven by cloud-top cooling (Wood, 2012). We have added this explanation to Section 4.4, together with the cloud-top height discussion in our response to Major Comment 3.

Reference

Wood, R., 2012. Stratocumulus Clouds. Mon. Weather Rev. 140, 2373–2423.

5. Given that WDM6_ICE improves LWC but substantially underestimates IWC, it would be useful to show the vertical profile of total condensate water content, e.g., LWC + total IWC, and/or the ice fraction. This would help evaluate whether WDM6_ICE improves the overall cloud water structure or mainly shifts condensate from ice to liquid. Such a diagnostic would also support the discussion of balanced phase partitioning and total water path biases.

: We have added a figure showing the vertical profiles of total condensate (LWC + IWC) and ice fraction along the flight track and at BAR (Fig. R6 of this response; added to the main text). Along the flight track, the observed ice fraction decreases from near unity at cloud base to about 0.04–0.09 in the upper cloud, indicating a liquid-dominated mixed-phase layer. WDM6 retains a high ice fraction of about 0.7–1.0 throughout the layer, whereas WDM6_ICE follows the observed decrease toward low values aloft, reaching about 0.01 above 900 m. The total condensate shows that WDM6 produces a near-negligible amount, while WDM6_ICE recovers a pronounced peak close to the observed magnitude. WDM6_ICE therefore recovers the total condensate toward the observed value, but the ice fraction shows that it does so by shifting almost entirely to the liquid phase, in contrast to the observed mixed-phase layer in which ice and liquid coexist. We have added this diagnostic and its description to Section 3.1.

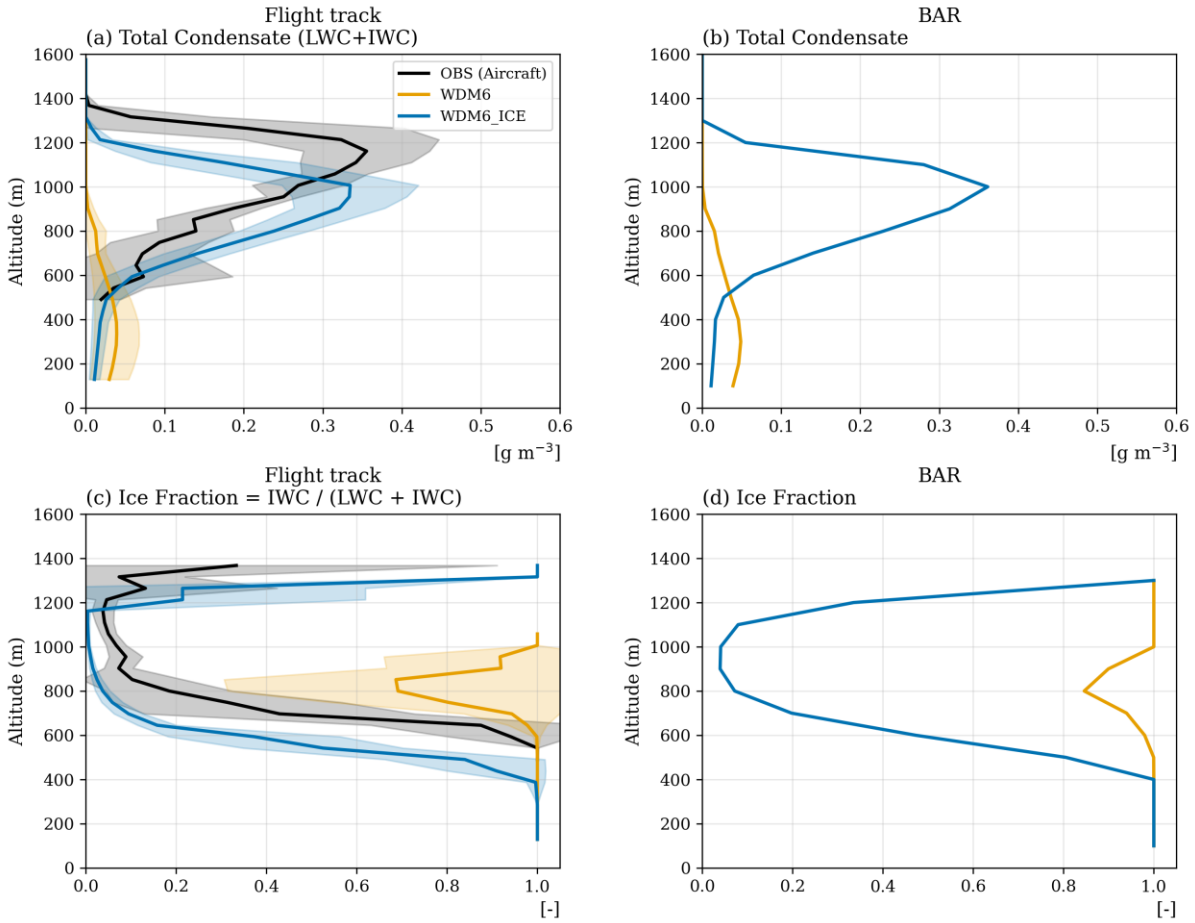

Figure R6: Vertical profiles of (a, b) total condensate (LWC + IWC) and (c, d) ice fraction (IWC / (LWC + IWC); IWC = qi + qs + qg). The left column (a, c) shows the profiles sampled along the flight track of Flight 10a during 01:00–02:00 UTC 10 October 2004, and the right column (b, d) shows the time-averaged (12:00 UTC 9 October – 11:00 UTC 10 October 2004) profiles at BAR. Black lines with gray shading indicate aircraft observations (01:10–02:00 UTC 10 October 2004; ±1σ). Colored lines denote model simulations: WDM6 (orange) and WDM6_ICE (blue).

6. Please clarify in the Fig. 6 caption whether model IWC is calculated consistently with Fig. 3, i.e., as the sum of cloud ice, snow, and graupel mixing ratios.

: We confirm that model IWC is calculated consistently in Figs. 3 and 6 as the sum of the cloud ice, snow, and graupel mixing ratios (q_i+q_s+q_g). We have clarified this in the Fig. 6 caption to match Fig. 3.

7. Line 330 ， Please use consistent capitalization for microphysical process names, e.g., PIDEP and PINUD/PNUD, and define each process clearly at first use.

: We have unified the capitalization of all microphysical process-rate names throughout the manuscript, including Line 330 and the figure captions. The process names now appear consistently as Pidep, Psdep, Pigen, Piacw, Pinud, Psacw, Pcond, Praut, Pracw, Psaut and Psaci, and each process is now defined at first use.

8. In the discussion of radiative biases, the authors should report the longwave and shortwave radiation biases relative to observations, rather than only the absolute

fluxes. Since Arctic MPCs strongly affect surface longwave radiation, the LWDOWN bias is particularly relevant for evaluating whether improved liquid water representation leads to improved surface energy balance.

: We have added the longwave and shortwave radiative biases relative to the observations directly in Table 3, given in parentheses next to the absolute fluxes (simulation − OBS). The revised Section 4.3 highlights that the longwave bias decreases from −43.3 W m^{-2} in WDM6 to −4.7 W m^{-2} in WDM6_ICE, with the intermediate-LWP configurations showing the smallest combined biases.